NATIONAL AERONAUTICS AND SPACE ADMINISTRATION

Technical Report 32-1287

Analysis of the Crushing of a Dovetail Phenolic Honeycomb Spherical Impact Limiter

A. C. Knoell

JET PROPULSION LABORATORY
CALIFORNIA INSTITUTE OF TECHNOLOGY
PASADENA, CALIFORNIA

July 1, 1968

NATIONAL AERONAUTICS AND SPACE ADMINISTRATION

Technical Report 32-1287

Analysis of the Crushing of a Dovetail Phenolic Honeycomb Spherical Impact Limiter

A. C. Knoell

Approved by:

for W. H. Gayman

M. E. Alper, Manager
Applied Mechanics Section

JET PROPULSION LABORATORY
CALIFORNIA INSTITUTE OF TECHNOLOGY
PASADENA, CALIFORNIA

July 1, 1968

TECHNICAL REPORT 32-1287

Prepared Under Contract No. NAS 7-100
National Aeronautics & Space Administration

Acknowledgment

The author wishes to acknowledge the work of Dr. R. R. Stephenson. His work was most useful in establishing much of the analytical approach used in this analysis.

Contents

Figures

Abstract

An analysis capability is developed to predict the static and dynamic crushing response of a Dovetail spherical impact limiter. The capability includes (1) a set of design relations to determine maximum limiter impact velocity and deceleration, (2) qualitative expressions to determine the effects of stress waves on limiter dynamic response, and (3) relations to establish the deceleration level at which payload "cannonballing," i.e., penetration of the payload sphere into the Dovetail limiter, occurs. Pertinent geometric and material assumptions are presented and the governing differential equation of motion is developed using principles of fluid mechanics.

Analysis of the Crushing of a Dovetail Phenolic Honeycomb Spherical Impact Limiter

I. Introduction

In the development of unmanned space vehicles, considerable emphasis has been placed on the development of energy-dissipating materials and devices capable of protecting scientific payloads during lunar or planetary landings. Conditions of omnidirectional impact have generally required that the payload configuration be spherical. This requirement has implied that the energy-dissipating mediums possess spherical curvature capability, thereby giving rise to an impact limiter configuration consisting of a spherical payload encased in an energy-dissipating shell.

A new type of nonhexagonal cell phenolic honeycomb possessing good spherical curvature capability and energy-dissipating characteristics has recently been developed (Ref. 1). This honeycomb, known as Dovetail, is shown schematically in Fig. 1. It has a constant cell foil thickness and consists of phenolic resin built up on a glass cloth core. The Dovetail is classified according to cell size, cell configuration, and bulk weight density.

An actual spherically curved specimen is shown in Fig. 2. This specimen has a curvature ratio R_p/d (payload radius/core thickness) of 1.8. This curvature capability represents an order of magnitude improvement in comparison to the best curving results obtained for hexagonal cell honeycomb (Ref. 2).

A. Objective and Scope

The purpose of this report is to present a method of theoretically predicting the static and dynamic response characteristics of a Dovetail phenolic honeycomb spherical impact limiter during vertical crushing against a flat unyielding surface. The static response includes the development of the crushing force as a function of the Dovetail material properties and limiter geometry, and the expression of this force in terms of the crushing depth. The dynamic response includes the determination of the maximum impact velocity and deceleration experienced by a Dovetail limiter. Included in the dynamic analysis are the effects of thickness efficiency (a parameter describing the limit of Dovetail crushability before "bottoming out" occurs) and stress waves generated by high velocity impact of the limiter. The so-called cannonball effect, i.e., the possible penetration of the payload sphere into the Dovetail honeycomb during impact, is considered by determining the deceleration limit at which this phenomenon occurs.

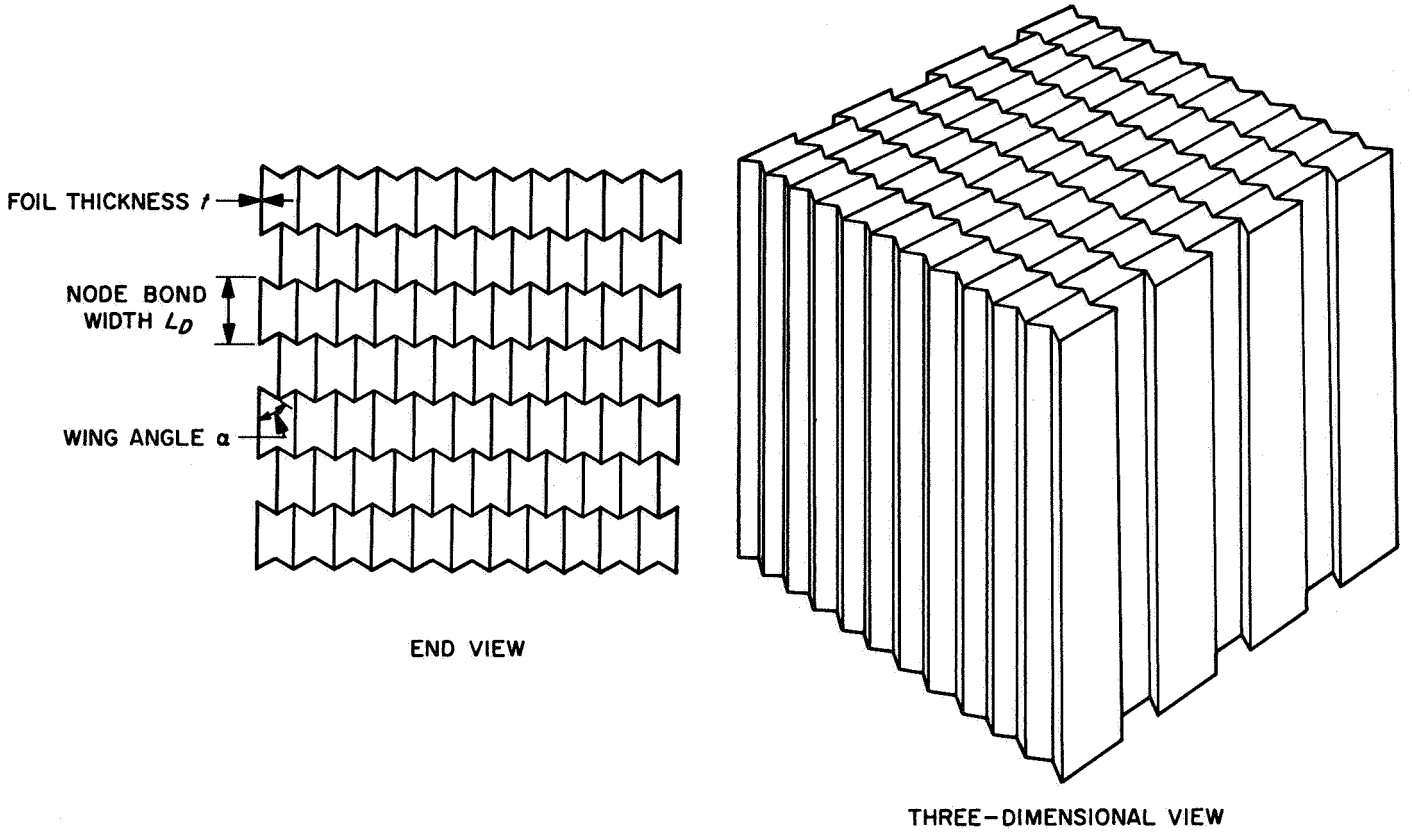

Fig. 1. Schematic of Dovetail honeycomb section

It is intended that this theoretical analysis be implemented in the future by comparing the mathematical force-displacement response characteristics of a Dovetail spherical limiter with actual test data. At that time, design charts based on the relations developed in this analysis will also be presented for specific Dovetail limiters. Finally, the analysis capability will be extended to include the effects of surface curvature on the energy-dissipating capability of a Dovetail spherical limiter.

B. Assumptions

In developing the limiter analytic model, it is assumed that the payload is a rigid body and that the cells of the Dovetail honeycomb are geometrically identical and uniformly distributed throughout the limiter. This latter assumption implies that spherical geometric symmetry exists and, as a consequence, there is no variation in circumferential bulk density of the Dovetail. For small Dovetail cell sizes, this assumption is valid since the honeycomb tends to approach a continuous medium. Also, since the Dovetail honeycomb is composed of small cell sizes, it is assumed that continuous functional theory applies. Finally, it is assumed that the Dovetail honeycomb is infinitely rigid in shear and that the only failure mode is crushing of the honeycomb.

Upon impact, it is assumed that the limiter is moving vertically with respect to a local, flat, rigid surface terrain and without rotation about its own gravity center. Thus, the impact kinetic energy is composed only of translational energy, and energy dissipation is provided solely by crushing of the Dovetail honeycomb.

C. Notation

During the deceleration process, the spherical Dovetail impact limiter will assume a general crushed configuration as shown in Fig. 3. The notation associated with this configuration, including additional pertinent parameters, is as follows:

R_p = payload radius

d = Dovetail core thickness

σ_{OB} = crushing stress at crushing boundary AB

A_{OB} = area at crushing boundary

ϕ = angular location of general Dovetail cell

$\theta = \phi_{max}$

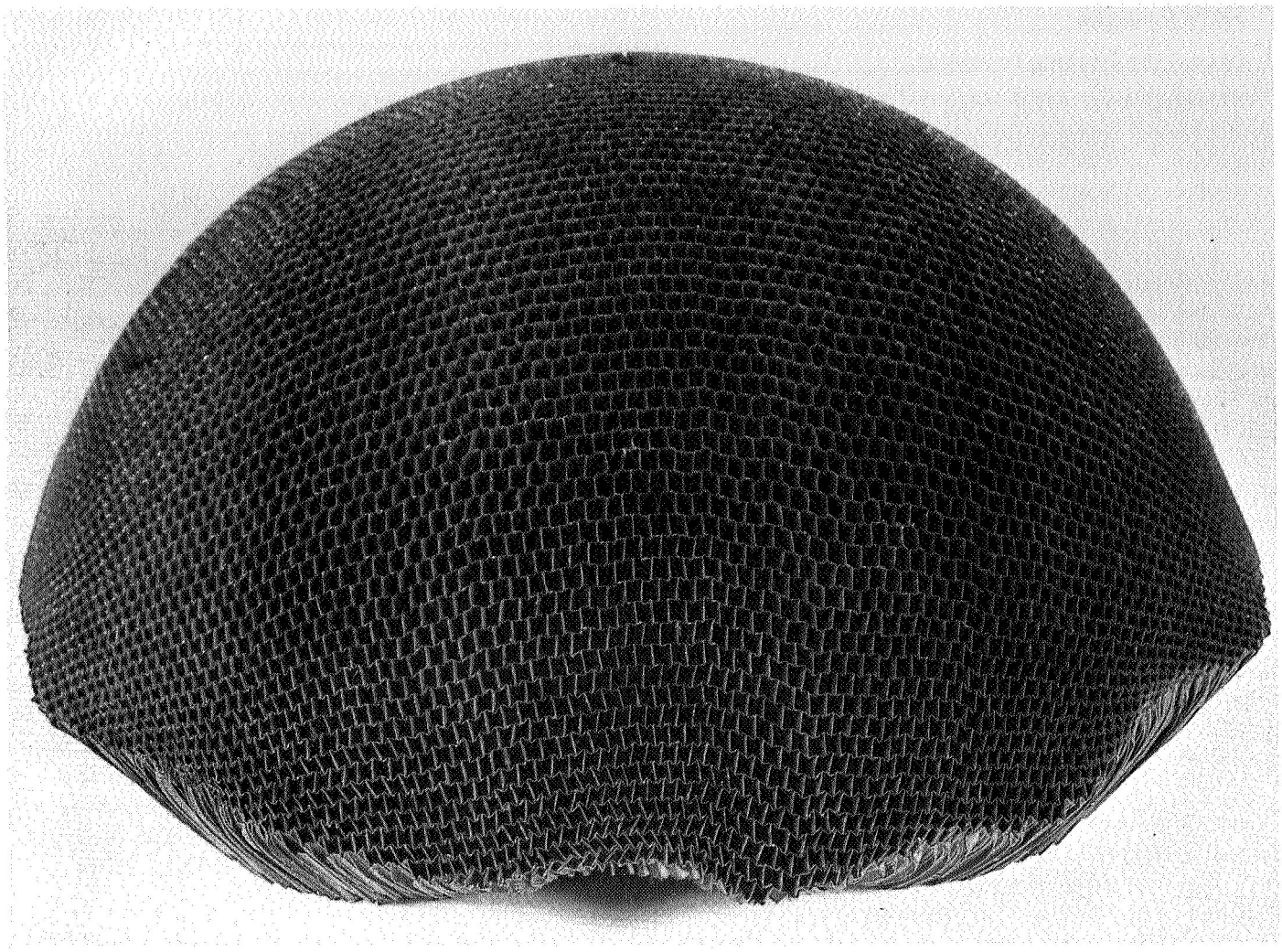

Fig. 2. Spherically curved Dovetail honeycomb specimen

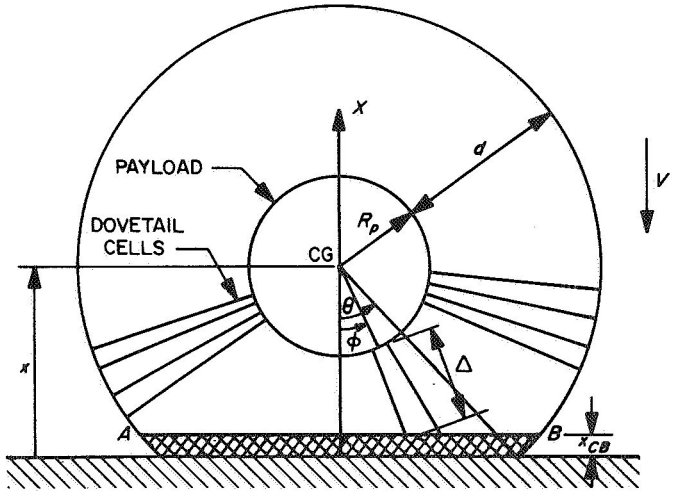

Fig. 3. Partially crushed Dovetail spherical impact limiter

Δ = length of general Dovetail cell

x = height of CG above crushing surface

x_{CB} = height of crushing boundary above crushing surface

V = impact limiter velocity

W_p = payload total weight

W_D = Dovetail total weight

η = payload fraction $\left(\frac{W_p}{W_p + W_D}\right)$

ρ_p = payload weight density

ρ_D = Dovetail weight density

a = cross-sectional area of Dovetail cell

II. Static Analysis

A. Force at the Crushing Boundary

1. General force relationship. As shown in Fig. 3, the impact limiter configuration consists of a small region of compressed particles that are at rest in a Newtonian reference frame, a boundary at which crushing of the Dovetail honeycomb is taking place, and of a region of particles that are above the crushing boundary and are in uniform vertical motion. However, the region of particles at rest represents only a very small but finite layer of crushed Dovetail particles. The majority of particles previously brought to rest split from the honeycomb material and are mostly contained within the hollow Dovetail cells. This crushing phenomenon ideally results in a flat crushing boundary rather than the spherical boundary developed during crushing of balsa wood impact limiters (Ref. 3).

Since $x_{CB} \simeq 0$, the force at the crushing boundary and the force at the limiter-surface interface are for all practical purposes identical. Thus, the force at the crushing boundary may be considered to be a function only of x rather than $x - x_{CB}$. This simplification geometrically facilitates the development of the force at the crushing boundary.

The force developed at the crushing boundary is of particular interest, since the area under the crushing force-displacement curve represents the maximum amount of kinetic energy that can be dissipated during the deceleration process. Since $x = x_{(\theta)}$, this force can be conveniently expressed by the relation:

$$F_{(\theta)} = \int_{AC_{(\theta)}} \sigma_{CB} dA \tag{1}$$

Equation (1) indicates that the total crushing force depends on the limiter geometry and crushing stress of the Dovetail honeycomb. The crushing stress at any point along the crushing boundary depends on the honeycomb bulk density, cell shape, and angle of loading of the Dovetail cell at that point. Data indicating the effect of these parameters on the axial crushing stress of Dovetail phenolic honeycomb have been experimentally developed and are contained in Ref. 1.

Since the effect of angle loading on the axial crushing stress of Dovetail is virtually insensitive to changes in material bulk density and cell shape, the crushing stress of Dovetail at the crushing boundary may be expressed as

$$\sigma_{CB} = \sigma_{0_{(\rho_D, a)}} \xi_{(\phi)} \tag{2}$$

where

σ_0 = axial crushing stress of Dovetail at density ρ_D and cell shape a

ξ = off-axis crushing stress reduction parameter

Based on experimental data, the polynomial expressions for σ_0 and ξ may be developed and substituted in Eq. (2). Recognizing that the ultimate objective is to substitute Eq. (2) in Eq. (1) and solve for $F_{(\theta)}$, it is convenient to express $\sigma_{CB} = \sigma_{CB(\phi,\theta)}$. In so doing, it is necessary to develop $a = a_{(\phi,\theta)}$ and $\rho_D = \rho_{D(\phi,\theta)}$. These relationships are developed below.

2. Cell shape. Figure 4 shows two views of a typical Dovetail cell in a spherically curved condition. The cell shape $a_{(\phi,\theta)}$ is described quantitatively through a relationship developed for the cross-sectional cell area. The cross-sectional area at cell length Δ is approximately trapezoidal and can be expressed as

$$a = \bar{y}(L_D + 2\bar{x}) \tag{3}$$

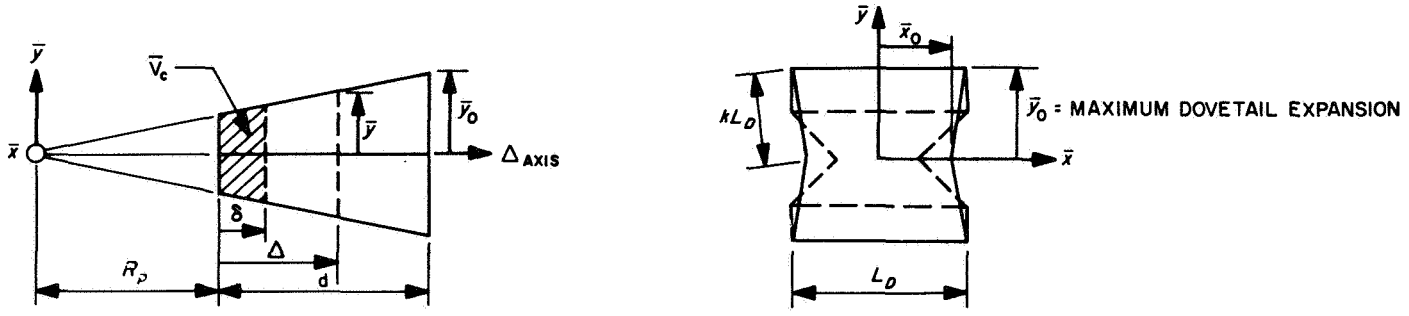

Fig. 4. Typical spherically curved Dovetail cell

But, by geometry

$$\bar{y} = \left(\frac{R_p + \Delta}{R_p + d}\right)\bar{y}_0 \tag{4}$$

Also, since the Dovetail cells are expanded in spherical curvature

$$\bar{y} = \bar{x} \tag{5}$$

Substituting Eqs. (4) and (5) in Eq. (3) yields

$$a = 2\bar{y}_0^2\left(\frac{R_p + \Delta}{R_p + d}\right)^2 + L_D\bar{y}_0\left(\frac{R_p + \Delta}{R_p + d}\right) \tag{6}$$

But, from the geometry shown in Fig. 3:

$$\cos\theta = \frac{x}{R_p + \Delta} \tag{7}$$

and

$$\cos\phi = \frac{x}{R_p + d} \tag{8}$$

Eliminating x from Eqs. (7) and (8) results in the expression

$$\Delta = R_p\left[\left(1 + \frac{1}{\frac{R_p}{d}}\right)\frac{\cos\theta}{\cos\phi} - 1\right] \tag{9}$$

Substituting Eq. (9) in Eq. (6) yields

$$a_{(\phi,\theta)} = 2\bar{y}_0^2\left(\frac{\cos\theta}{\cos\phi}\right)^2 + L_D\bar{y}_0\left(\frac{\cos\theta}{\cos\phi}\right) \tag{10}$$

3. Dovetail weight density. The weight per unit volume of Dovetail honeycomb surrounding the payload sphere is defined as the Dovetail weight density. Since the honeycomb material is composed of individual cells having constant unit weight along the cell axis, a radial variation in Dovetail density exists. This variation does not exist in the homogeneous impact limiters such as those containing balsa wood as the energy-dissipating material.

Considering a shell of Dovetail honeycomb having a core thickness Δ, it follows that the Dovetail density may be expressed as:

$$\rho_{D(\Delta)} = \frac{W_{(\Delta)}}{V_{(\Delta)}} = \frac{W_{(\Delta)}}{\frac{4}{3}\pi\left[(R_p + \Delta)^3 - R_p^3\right]} \tag{11}$$

Since the Dovetail unit cell weight is constant,

$$W_{(\Delta)} = \left(\frac{\Delta}{d}\right)W_D \tag{12}$$

Thus, Eq. (11) becomes

$$\rho_{D(\Delta)} = \frac{3W_D}{4\pi d\left(3R_p^2 + 3R_p\Delta + \Delta^2\right)} \tag{13}$$

Substituting Eq. (9) in Eq. (13) yields

$$\rho_{D(\phi,\theta)} = \frac{3W_D}{4\pi R_p^2 d\left\{\left(1 + \frac{1}{\frac{R_p}{d}}\right)\left(\frac{\cos\theta}{\cos\phi}\right)\left[\left(1 + \frac{1}{\frac{R_p}{d}}\right)\left(\frac{\cos\theta}{\cos\phi}\right) + 1\right] + 1\right\}} \tag{14}$$

Eqs. (10) and (14) represent transformation relations for converting the polynomial expression for $\sigma_{0_{(\rho_D,\alpha)}}$ to $\sigma_{0_{(\phi,\theta)}}$.

4. Differential limiter area. It now remains to determine $dA = dA_{(\phi,\theta)}$ such that the integral expression for $F_{(\theta)}$ may be completely established. From the geometry of Fig. 3, it can readily be shown that

$$dA = \pi\left(R_p + d\right)^2\cos^2\theta\left[\tan^2\left(\phi + d\phi\right) - \tan^2\phi\right] \tag{15}$$

Solving Eq. (15), neglecting higher order terms, yields

$$dA_{(\phi,\theta)} = 2\pi R_p^2\left(1 + \frac{1}{\frac{R_p}{d}}\right)^2\left(\frac{\cos^2\theta\sin\phi}{\cos^3\phi}\right)d\phi \tag{16}$$

5. Final force relationship. Substituting Eq. (2) (transformed) and Eq. (16) in Eq. (1) yields

$$F_{(\theta)} = 2\pi R_p^2\left(1 + \frac{1}{\frac{R_p}{d}}\right)^2\int_0^{\theta}\sigma_{0_{(\phi,\theta)}}\dot{\xi}_{(\phi)}\left(\frac{\cos^2\theta\sin\phi}{\cos^3\phi}\right)d\phi \tag{17}$$

Equation (17) presents the crushing force in a form that is more convenient for a subsequent dynamic analysis. However, the static crushing force-displacement profile may be constructed from this equation by transforming

the independent variable θ to crushing depth d_C. By geometry (Fig. 3) the crushing depth can be expressed as:

$$d_C = (R_p + d) - x \tag{18}$$

Substituting Eq. (9) in Eq. (18) yields

$$d_C = (R_p + d)(1 - \cos\theta) \tag{19}$$

Equation (19) represents the transformation equation whereby $F = F_{(d_C)}$ can be developed.

B. Thickness Efficiency Effect

During crushing of the Dovetail honeycomb, a crushing depth will be reached at which a marked increase in force is required to continue the crushing process. In a design sense, this crushing depth, which characterizes the onset of the "bottoming-out" region of the force-displacement diagram, represents the useful stroke limit of the honeycomb core. The ratio of this useful stroke limit to the honeycomb core thickness is defined as thickness efficiency β. It is this parameter that controls the maximum value of θ (for a given R_p/d ratio), which can be used in Eq. (17).

In the case of Dovetail honeycomb, "bottoming-out" will occur when the crushed particles completely fill the centrally-loaded cell cavity. Thus, as an approximation for the thickness efficiency β, it follows from the geometry of Fig. 4 that

$$\overline{V}_C = \int_0^{\delta} a_{(\Delta)}\, d\Delta \,(\text{geometric volume})$$

$$= \frac{t_f}{2}(d - \delta)(2L_D + 4kL_D)\,(\text{crushed particle volume}) \tag{20}$$

where

t_f = Dovetail (wing) foil thickness

Then from Eq. (6),

$$\int_0^{\delta}\left[2\bar{y}_0^2\left(\frac{R_p + \Delta}{R_p + d}\right)^2 + L_D\bar{y}_0\left(\frac{R_p + \Delta}{R_p + d}\right)\right]d\Delta = t_f dL_D\left(1 - \frac{\delta}{d}\right)(1 + 2k) \tag{21}$$

Letting $K = [1 + (R_p/d)]$ and recognizing that $\beta = [1 - (\delta/d)]$, Eq. (21) becomes, after integration,

$$\bar{y}_0 K\left\{\frac{2\bar{y}_0}{3}\left[\left(1 - \frac{\beta}{K}\right)^3 + \left(\frac{1-K}{K}\right)^3\right] + \frac{L_D}{2}\left[\left(1 - \frac{\beta}{K}\right)^2 - \left(\frac{1-K}{K}\right)^2\right]\right\} = L_D t_f \beta(1 + 2k) \tag{22}$$

Rearranging terms and letting

$$Z = \left(1 - \frac{\beta}{K}\right) \tag{23}$$

Eq. (22) becomes

$$Z^3 + \left(\frac{3L_D}{4\bar{y}_0}\right)Z^2 + \frac{3L_D t_f}{2\bar{y}_0^2}(1 + 2k)Z + \left(\frac{1-K}{K}\right)^3 - \frac{3L_D}{4\bar{y}_0}\left(\frac{1-K}{K}\right)^2 - \frac{3t_f L_D}{2\bar{y}_0^2}(1 + 2k) = 0 \tag{24}$$

The number of unknowns in Eq. (24) can be reduced by one by eliminating the factor k. This reduction is done by considering the Dovetail cell geometry shown in Fig. 4. For any curvature, it is clear that at the Dovetail outer surface

$$k^2 L_D^2 = \left(\frac{L_D}{2} - \bar{x}_0\right)^2 + \bar{y}_0^2 \tag{25}$$

But for spherical curvature ($\bar{x}_0 = \bar{y}_0$), Eq. (25) becomes

$$k^2 L_D^2 = \left(\frac{L_D}{2} - \bar{y}_0\right)^2 + \bar{y}_0^2 \tag{26}$$

Solving for k:

$$k = 0.353\left[1 + \left(\frac{4\bar{y}_0}{L_D} - 1\right)^2\right]^{1/2} \tag{27}$$

Substituting Eq. (27) in Eq. (24) yields

$$Z^3 + \left(\frac{3L_D}{4\bar{y}_0}\right)Z^2 + \frac{3L_D t_f}{2\bar{y}_0^2}\left\{1 + 0.706\left[1 + \left(\frac{4\bar{y}_0}{L_D} - 1\right)^2\right]^{1/2}\right\}Z + \left(\frac{1-K}{K}\right)^3 - \frac{3L_D}{4\bar{y}_0}\left(\frac{1-K}{K}\right)^2 - \frac{3L_D t_f}{2\bar{y}_0^2}\left\{1 + 0.706\left[1 + \left(\frac{4\bar{y}_0}{L_D} - 1\right)^2\right]^{1/2}\right\} = 0 \tag{28}$$

Although Eq. (28) is cubic in Z, only one positive real solution exists as is evident from a physical interpretation of Fig. 4. The value of thickness efficiency can then be obtained by substituting the solution of Eq. (28) in Eq. (23) and solving for β.

To determine the maximum value of θ, it is seen from Eq. (8) that letting $x = R_p + \delta$:

$$\cos\theta_{MAX} = \frac{R_p + \delta}{R_p + d} \tag{29}$$

But from the expressions for β and K, Eq. (29) may be rewritten as

$$\cos\theta_{MAX} = \frac{K - \beta}{K} = 1 - \frac{\beta}{K} = Z$$

$$\therefore \theta_{MAX} = \cos^{-1}(Z) \tag{30}$$

Thus, Eq. (17) is valid in the region

$$0 \leq \theta \leq \theta_{MAX}$$

III. Dynamic Analysis

A. Governing Differential Equation of Motion

1. Derivation of equation of motion. To properly account for the stopped mass effect on the deceleration of a Dovetail phenolic honeycomb impact limiter, it is convenient to develop the equation of motion governing the deceleration process from principles of fluid mechanics. Specifically, the development is based on application of Newton's second law to a system or particles contained within a control volume that is accelerating and has mass crossing its boundaries.

Such a system of particles and control volume is shown in Fig. 5. Since the impact of the Dovetail limiter is vertical, only motion along an axis parallel to the velocity vector is considered.

where

$\overline{V}$ = control volume

S = system of particles

v = particle velocity

ρ = particle mass density

u = velocity of mass transfer boundary

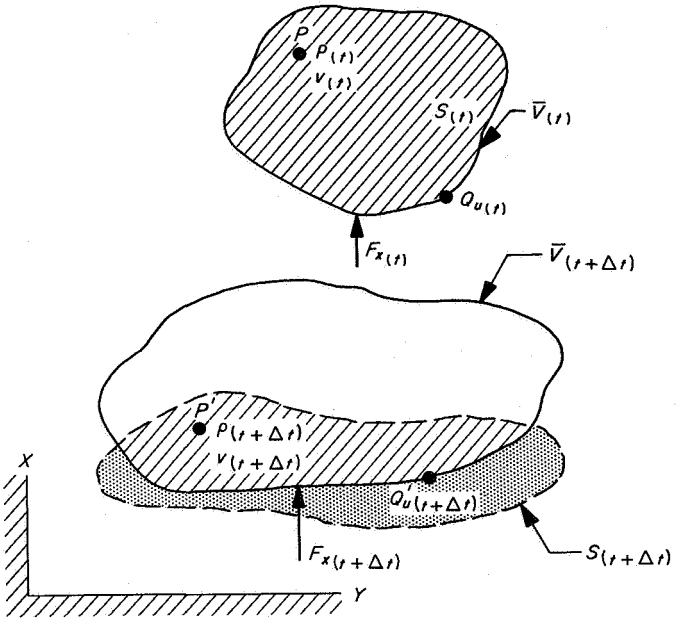

Fig. 5. System of particles and control volume

F_x = force acting on system of particles

P = general particle within control volume

Q = general point on control volume boundary

Newton's second law states that

$$F_{x(t)} = \frac{d}{dt}\{M_{x(t)}\} = \lim_{\Delta t \to 0}\left\{\frac{M_{x(t+\Delta t)} - M_{x(t)}}{\Delta t}\right\} \tag{31}$$

where M_x = linear momentum of system of particles in X direction.

Since the control volume and the system of particles coincide at time t, the linear momentum represents simply the sum of all particle momenta within the control volume. Thus,

$$M_{x(t)} = \int_{\overline{V}_{(t)}} \rho_{(t)} v_{(t)} d\overline{V} \tag{32}$$

At time $t + \Delta t$, the control volume and the system of particles within the control volume change to $\overline{V}_{(t+\Delta t)}$ and $S_{(t+\Delta t)}$, respectively. As the particle system changes, mass flows across the boundary of the control volume. This mass flow gives rise to a momentum flux that must be accounted for in the expression for linear momentum

in addition to the particle momenta within the control volume. Thus, the expression for $M_{x_{(t+\Delta t)}}$ may be written as

$$M_{x_{(t+\Delta t)}} = \int_{\overline{V}_{(t+\Delta t)}} \rho_{(t+\Delta t)} v_{(t+\Delta t)} d\overline{V} - \int_{A_{(t+\Delta t)}} \left(\frac{\rho_{(t+\Delta t)} + \rho_{(t)}}{2}\right)\left(\frac{v_{(t+\Delta t)} + v_{(t)}}{2}\right) \times \left[\left(\frac{(v-u)_{(t+\Delta t)} + (v-u)_{(t)}}{2}\right)\left(\frac{dA_{(t+\Delta t)} + dA_{(t)}}{2}\right)\Delta t\right] \tag{33}$$

The surface integral of Eq. (33) represents a linear average of the momentum flux crossing the control volume boundary during the time interval Δt. As $\Delta t \to 0$, this average approaches the true momentum flux. The negative sign in front of the surface integral indicates that mass is leaving the control volume.

Substituting Eqs. (32) and (33) in Eq. (31) and passing to the limit yields

$$F_{x_{(t)}} = \frac{\partial}{\partial t}\int_{\overline{V}_{(t)}} \rho v \, d\overline{V} - \int_{A_{(t)}} \rho v (v-u) \, dA \tag{34}$$

Equation (34) is known as the momentum theorem and agrees with the vector formulation presented in Ref. 4.

The equation of motion governing the deceleration of the Dovetail honeycomb impact limiter can now be determined by applying Eq. (34) to the system of particles within the control volume above the crushing boundary *AB*, shown in Fig. 3.

The left-hand side of Eq. (34) represents the force acting at the crushing boundary. This force is a function of the impact limiter geometry and Dovetail material properties, and has been developed as a function of θ in Eq. (17).

The right-hand side of Eq. (34) consists of a volume and surface integral. With the assumption that all particles within the control volume have the same velocity (thereby neglecting stress wave effects), the volume integral becomes

$$\int_{\overline{V}_{(t)}} \rho v \, d\overline{V} = v \int_{\overline{V}_{(t)}} \rho \, d\overline{V} = \dot{x} \int_{\overline{V}_{(t)}} \rho \, d\overline{V} \tag{35}$$

The particle velocity $v_{(t)}$, which is now the same as the impact limiter velocity $\dot{x}_{(t)}$ (Fig. 3), appears outside the integral since it does not depend on location within the control volume.

But,

$$\int_{\overline{V}_{(t)}} \rho \, d\overline{V} = m_{UC} \tag{36}$$

where m_{UC} = uncrushed mass of the impact limiter. Thus, Eq. (35) becomes

$$\int_{\overline{V}_{(t)}} \rho v \, d\overline{V} = m_{UC} \dot{x} \tag{37}$$

By the same reasoning, the surface integral of Eq. (34) becomes

$$\int_{A_{(t)}} \rho v (v-u) \, dA = \dot{x}(\dot{x} - \dot{x}_C) \int_{A_{(t)}} \rho \, dA \tag{38}$$

Substituting Eqs. (37) and (38) in Eq. (34) and differentiating yields

$$F_x = m_{UC}\ddot{x} + \dot{x}\frac{\partial}{\partial t}(m_{UC}) - \dot{x}(\dot{x} - \dot{x}_C)\int_{A_{(t)}} \rho \, dA \tag{39}$$

The surface integral of Eq. (39) can now be considered as the integral of the Dovetail bulk mass density over the area at the crushing boundary A_{CB}. Since the density depends on location within A_{CB}, the integral of the density distribution over the area at the crushing boundary is equivalent to some average density multiplied by the same area. Thus,

$$\int_{A_{(t)}} \rho \, dA = \rho_{AVG} A_{CB} \tag{40}$$

From Fig. 3, it is clear that m_{UC} can be expressed as

$$m_{UC} = \left(\frac{W_p + W_D}{g}\right) - \int_{\overline{V}_{C_{(t)}}} \rho \, d\overline{V}_C \tag{41}$$

where

$\overline{V}_C$ = crushed volume of the sphere

g = gravitational constant

Then,

$$\frac{\partial}{\partial t}(m_{UC}) = -\frac{\partial}{\partial t}\left[\int_{\overline{V}_{C_{(t)}}} \rho \, d\overline{V}_C\right] \tag{42}$$

Also, from the geometry shown in Fig. 3, it is possible to express the volume integral of Eq. (42) as

$$I = \int_{\overline{V}_{C(t)}} \rho \, d\overline{V}_C$$

$$= \int_{(x-x_{CB})}^{(R_p+d)} \rho_{AVG(x-x_{CB})} A_{CB(x-x_{CB})} \, d(x - x_{CB}) \qquad (43)$$

now

$$\frac{\partial I}{\partial t} = \frac{\partial I}{\partial (x - x_C)} \frac{\partial (x - x_C)}{\partial t}$$

$$\therefore \frac{\partial I}{\partial t} = -\rho_{AVG} A_{CB} (\dot{x} - \dot{x}_C)$$

Thus, Eq. (42) becomes

$$\frac{\partial m_{UC}}{\partial t} = (\dot{x} - \dot{x}_C) \rho_{AVG} A_C \qquad (44)$$

Substituting Eqs. (40) and (44) in Eq. (39) yields

$$F_x = m_{UC} \ddot{x} \qquad (45)$$

Equation (45) is the differential equation of motion governing the deceleration of a Dovetail honeycomb impact limiter. It represents the kinetic relationship between the force at the crushing boundary and the deceleration experienced by the impact limiter.

A relationship* identical to that given by Eq. (45) was developed in an analysis of an omnidirectional impact limiter. The derivation approach was similar to that used above; however, the energy-dissipating material was considered to be homogeneous with no radial variation in bulk density.

2. *Solution of equation of motion.* Equation (45) may now be solved to determine the maximum impact velocity and deceleration of a spherical Dovetail honeycomb impact limiter. Noting that F, m_{UC}, and the limiter velocity V can be expressed as functions of displacement, Eq. (45) can be reduced to a first order differential equation as follows:

$$\frac{F}{m_{UC}} = \ddot{x} = \frac{dV}{dt} = V \frac{dV}{dx}$$

$$\therefore V dV = \frac{F}{m_{UC}} dx \qquad (46$$

Integrating Eq. (46) between the initial and final limits of velocity and displacement results in

$$\int_{V_i}^{V_f} V dV = \int_{x_i}^{x_f} \left(\frac{F}{m_{UC}}\right) dx \qquad (47)$$

From Fig. 3 it can be seen that the maximum impact velocity is the initial contact velocity V_i; and that for full utilization of the energy-dissipating material (Dovetail), bottoming-out should occur just as the limiter is brought to rest. Incorporating these characteristics in Eq. (47) and recalling that $F_x = F_{CB}$ since $x_{CB} = 0$ results in

$$\int_{V_0}^{0} V dV = \int_{(R_p+d)}^{R_p+(1-\beta)d} \left(\frac{F}{m_{UC}}\right)_x dx \qquad (48)$$

Integrating the left-hand side of Eq. (48) yields

$$V_0^2 = -2 \int_{(R_p+d)}^{R_p+(1-\beta)d} \left(\frac{F}{m_{UC}}\right)_x dx \qquad (49)$$

Using Eqs. (8) and (30), Eq. (49) may also be written as

$$V_0^2 = 2(R_p + d) \int_0^{\theta_{MAX}} \left(\frac{F}{m_{UC}}\right)_\theta \sin\theta \, d\theta \qquad (50)$$

The crushing force F has been developed as $F_{(\theta)}$ in Eq. (17), and may be substituted directly in Eq. (50). In developing $m_{UC(\theta)}$, the following weight balance equation applies:

$$m_{UC} g = (W_p + W_D) - W_C \qquad (51)$$

where W_C = Dovetail honeycomb crushed weight. Consider now the spherical limiter segment shown in Fig. 6. For the elemental volume slice

$$dW_C = 2\pi \rho_{D(r,x)} r \, dr \, dx$$

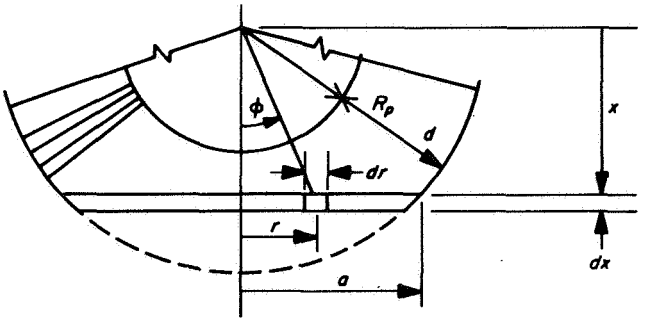

Fig. 6. Crushed segment of Dovetail impact limiter

*JPL Internal Communication by Dr. R. R. Stephenson.

Then,

$$W_C = 2\pi \int_x^{(R_p+d)} \int_0^a \rho_{D_{(r,x)}}\, r\, dr\, dx \tag{52}$$

But, by geometry

$$r = x \tan\phi \qquad x = (R_p + d)\cos\theta$$

$$dr = x \sec^2\phi\, d\phi \qquad dx = (R_p + d)\sin\theta\, d\theta \tag{53}$$

Then, combining these relations gives

$$r = (R_p + d)\cos\theta \tan\phi \tag{54}$$

$$dr = (R_p + d)\cos\theta \sec^2\phi\, d\phi \tag{55}$$

Substituting Eqs. (53), (54), and (55) in Eq. (52) and changing the limits of integration yields

$$W_C = 2\pi (R_p + d)^3 \int_0^\theta \sin\theta \cos^2\theta \int_0^\theta \rho_{D(\phi,\theta)} \tan\phi \sec^2\phi\, d\phi\, d\theta \tag{56}$$

Substituting Eq. (14) in Eq. (56) and the resulting equation in Eq. (51) yields

$$m_{UC}\, g = (W_p + \dot{W}_D) - \frac{3}{2}\left(\frac{R_p}{d}\right)\left(1 + \frac{1}{\frac{R_p}{d}}\right)^3 \times \int_0^\theta \sin\theta \cos^2\theta \int_0^\theta \frac{W_D \tan\phi \sec^2\phi}{\left\{\left(1 + \frac{1}{\frac{R_p}{d}}\right)\left(\frac{\cos\theta}{\cos\phi}\right)\left[\left(1 + \frac{1}{\frac{R_p}{d}}\right)\left(\frac{\cos\theta}{\cos\phi}\right) + 1\right] + 1\right\}} d\phi\, d\theta \tag{57}$$

Substituting Eqs. (17) and (57) in Eq. (50) yields

$$V_0^2 = 2R_p\left(1 + \frac{1}{\frac{R_p}{d}}\right) g \times \int_0^{\theta_{MAX}} \left[\frac{2\pi R_p^2 \left(1 + \frac{1}{\frac{R_p}{d}}\right)^2 \int_0^\theta \sigma_{0_{(\phi,\theta)}}\, \xi_{(\phi)} \left(\frac{\cos^2\theta \sin\phi}{\cos^3\phi}\right) d\phi}{(W_p + W_D) - \frac{3}{2}\left(\frac{R_p}{d}\right)\left(1 + \frac{1}{\frac{R_p}{d}}\right)^3 \int_0^\theta \sin\theta \cos^2\theta \int_0^\theta \frac{W_D \tan\phi \sec^2\phi}{\left\{\left(1 + \frac{1}{\frac{R_p}{d}}\right)\left(\frac{\cos\theta}{\cos\phi}\right)\left[\left(1 + \frac{1}{\frac{R_p}{d}}\right)\left(\frac{\cos\theta}{\cos\phi}\right) + 1\right] + 1\right\}} d\phi\, d\theta} \right] \times \sin\theta\, d\theta \tag{58}$$

The maximum value of the bracketed portion of the integrand of Eq. (58) is the maximum deceleration $\ddot{x}_L$ (in number of gs) of a Dovetail phenolic honeycomb spherical impact limiter. The corresponding solution of Eq. (58) yields the maximum impact velocity for the same Dovetail limiter.

B. Stress Waves—Qualitative Effect on Dynamic Response

Equation (58) represents the solution of the differential equation of motion governing the *average* deceleration of a Dovetail phenolic honeycomb impact limiter. Only the average dynamic response characteristics are predicted by Eq. (58), since Eq. (45) neglects stress variations during crushing due to stress wave reversals. However, as the number of stress wave reversals increases, the solution as given by Eq. (58) becomes more satisfactory, since it is based on an integrated deceleration effect. Thus, a qualitative measure of the stress wave effect on the dynamic response of a Dovetail impact limiter during crushing may be obtained by developing an expression for the number of stress wave reversal cycles occurring in the total time required to stop the limiter. Since no exact lower bound can be established for the number of stress wave reversal cycles below which stress wave effects must be considered, it is arbitrarily assumed that the solution as given by Eq. (58) is satisfactory, provided ten or more cycles occur.

Considering only the centrally loaded Dovetail cell, the number of stress wave reversal cycles is given by the relation

$$N = T\left(\frac{c}{2d}\right) \tag{59}$$

where

T = total limiter stopping time

c = stress wave velocity along a Dovetail cell

It should be noted that Eq. (59) will give a conservative (lower) estimate of the number of stress wave reversal cycles, since the distance over which the wave travels is considered constant and equal to the Dovetail core depth d. Actually, the height of the centrally loaded cell diminishes during crushing, thereby, permitting more reversals to occur. Only the centrally loaded cell is considered, since it represents the region of highest stress wave intensity.

Now, using the more conservative (lower bound) material properties of phenolic resin rather than glass, the stress wave velocity c can be expressed as (see Ref. 5):

$$c = \left(\frac{E}{\rho}\right)^{1/2} = \left(\frac{E_p g}{\gamma_p}\right)^{1/2} \tag{60}$$

where

E_p = modulus of elasticity of phenolic resin

γ_p = weight density of phenolic resin

Substituting Eq. (60) in Eq. (59) yields

$$N = \frac{T}{2d}\left(\frac{E_p g}{\gamma_p}\right)^{1/2} \tag{61}$$

To determine the total stopping time T, use is made of Eq. (46) with the right-hand side expressed in terms of θ. Thus,

$$V dV = \left(\frac{F}{m_{UC}}\right)_\theta dx_{(\theta)} \tag{62}$$

Differentiating Eq. (8) and substituting the result in Eq. (62) yields

$$V dV = -\left(\frac{F}{m_{UC}}\right)_\theta (R_p + d)\sin\theta\, d\theta \tag{63}$$

Recognizing that $w_{UC} = m_{UC} g$, Eq. (63) then becomes

$$V dV = -g\left(\frac{F}{w_{UC}}\right)_\theta (R_p + d)\sin\theta\, d\theta \tag{64}$$

Applying limits of integration to Eq. (64) gives

$$\int_{V_0}^{V} V dV = -g(R_p + d)\int_0^\theta \left(\frac{F}{w_{UC}}\right)_\theta \sin\theta\, d\theta$$

and integrating the left-hand side yields

$$V_{(\theta)} = \left[V_0^2 - 2g(R_p + d)\int_0^\theta \left(\frac{F}{w_{UC}}\right)_\theta \sin\theta\, d\theta\right]^{1/2} \tag{65}$$

Now, using the derivative of Eq. (8),

$$V = \frac{dx}{dt} = \frac{-(R_p + d)\sin\theta\, d\theta}{dt}$$

$$\therefore dt = \frac{-(R_p + d)\sin\theta}{V_{(\theta)}} d\theta \tag{66}$$

Substituting Eq. (65) in Eq. (66) and integrating yields

$$T = \int_0^{\theta_{MAX}} \frac{-(R_p + d)\sin\theta\, d\theta}{\left[V_0^2 - 2g(R_p + d)\int_0^{\theta}\left(\frac{F}{w_{UC}}\right)_{\theta}\sin\theta\, d\theta\right]^{1/2}} \tag{67}$$

Substituting Eq. (67) in Eq. (61) yields

$$N = \frac{1}{2}\left(\frac{R_p}{d}\right)\left(1 + \frac{1}{\frac{R_p}{d}}\right)\left(\frac{E_p g}{\gamma_p}\right)^{1/2} \times \int_0^{\theta_{MAX}} \frac{-\sin\theta\, d\theta}{\left[V_0^2 - 2g R_p\left(1 + \frac{1}{\frac{R_p}{d}}\right)\int_0^{\theta}\left(\frac{F}{w_{UC}}\right)_{\theta}\sin\theta\, d\theta\right]^{1/2}} \tag{68}$$

As $\theta \to \theta_{max}$, the denominator of the integrand of Eq. (68) approaches 0, which implies that $N \to \infty$. To arrive at a finite numerical solution to Eq. (68) and still maintain conservative results, arbitrarily let

$$0 < \theta < 0.95\theta_{max}$$

Thus, Eq. (68) becomes

$$N = \frac{1}{2}\left(\frac{R_p}{d}\right)\left(1 + \frac{1}{\frac{R_p}{d}}\right)\left(\frac{E_p g}{\gamma_p}\right)^{1/2} \times \int_0^{0.95\theta_{MAX}} \frac{-\sin\theta\, d\theta}{\left[V_0^2 - 2g R_p\left(1 + \frac{1}{\frac{R_p}{d}}\right)\int_0^{\theta}\left(\frac{F}{w_{UC}}\right)_{\theta}\sin\theta\, d\theta\right]^{1/2}} \tag{69}$$

Another measure of the stress wave effect on the dynamic response of a Dovetail limiter is afforded by consideration of the stress wave intensity at the payload-Dovetail interface. Since this interface is effectively a rigid joint, a compression wave traveling along the centrally loaded cell will reflect as a compression wave and double in intensity. Thus, assuming no dispersion of the axial wave and neglecting curvature effects at the interface, it may be conservatively stated that crushing of the Dovetail at the interface will not occur due to stress waves, provided

$$\frac{\sigma_{C_i}}{\sigma_{C_0}} > 2$$

where

σ_{C_i} = axial crushing stress of Dovetail at the payload-Dovetail interface

σ_{C_0} = axial crushing stress of Dovetail at the outer surface

C. Payload Penetration—"Cannonball" Effect

During the deceleration process, it is possible for the stress developed at the payload-Dovetail interface for a given impact limiter to exceed the crushing stress of the Dovetail honeycomb. If this condition occurs, the payload will penetrate the honeycomb material. Clearly, this behavior is undesirable, since only a small amount of Dovetail will be crushed (and, therefore, a small amount of kinetic energy dissipated) in a region where a significantly larger amount of Dovetail is available.

To provide a design check against possible payload penetration of the Dovetail, an expression for the maximum payload deceleration at which this phenomenon occurs will now be developed. The value of the maximum payload deceleration as predicted by this expression may then be compared to that of the maximum limiter deceleration as given by Eq. (58) to ensure that the former does not equal or exceed the latter.

Neglecting the contribution of the tensile strength of the upper half of the Dovetail sphere (Fig. 3) to the total force resisting payload penetration, the equation of monition governing the payload deceleration process can conservatively be written as

$$\left(\frac{W_p}{g}\right)\ddot{x}_p = P_C \tag{70}$$

where

P_C = compressive force acting on the payload below the equator

$\ddot{x}_p$ = payload deceleration

But, for maximum payload deceleration

$$P_C = \int_0^{\pi/2} \sigma_{C_i}\, \xi_{(\phi)}\, dA_{(\phi)} \tag{71}$$

Substituting Eq. (71) in Eq. (70) yields

$$\left(\frac{W_p}{g}\right)\ddot{x}_{p_{MAX}} = \int_0^{\pi/2} \sigma_{C_i}\, \xi_{(\phi)}\, dA_{(\phi)} \tag{72}$$

From the geometry of Fig. 3, it can be shown that at the payload-Dovetail interface

$$dA_{(\phi)} = 2\pi R_p^2 \sin\phi\, d\phi \tag{73}$$

Substituting Eq. (73) in Eq. (72) yields

$$\ddot{x}_{p_{MAX}} = \frac{2\pi R_p^2\, g\, \sigma_{C_i}}{W_p} \int_0^{\pi/2} \xi_{(\phi)} \sin\phi\, d\phi \tag{74}$$

From Eqs. (58) and (74), it is clear that payload penetration of the Dovetail honeycomb will not occur provided

$$\frac{\ddot{x}_{p_{MAX}}}{x_L} > 1$$

D. Design Relations

1. Relations independent of limiter weight. Introducing the concept of a payload fraction as defined in Section I-C, it is possible to develop a set of design relations that are independent of the impact limiter mass. These relations consist of expressions for maximum impact velocity, levels of constant deceleration, and impact limiter size as functions of the payload fraction and a given set of geometric and material limiter constants. Relationships of this type significantly reduce the number of cases to be analyzed for design purposes. In developing these relations, it is convenient to express the payload and Dovetail weights as follows:

$$W_p = \frac{4}{3}\pi R_p^3 \rho_p \tag{75}$$

and

$$W_D = \frac{4}{3}\pi\left[(R_p + d)^3 - R_p^3\right]\rho_{D_0} \tag{76}$$

where

ρ_{D_0} = Dovetail weight density at outer surface

Solving Eq. (76) for d gives

$$d = \left[\frac{3W_D}{4\pi\rho_{D_0}} + R_p^3\right]^{1/3} - R_p \tag{77}$$

But, by the definition of the payload fraction,

$$W_D = \left(\frac{1-\eta}{\eta}\right)W_p \tag{78}$$

Substituting Eq. (75) in Eq. (78) and the resulting equation in Eq. (77) yields

$$\frac{R_p}{d} = \frac{1}{\left[\frac{\rho_p}{\rho_{D_0}}\left(\frac{1-\eta}{\eta}\right)+1\right]^{1/3} - 1} \tag{79}$$

and

$$\left(1 + \frac{1}{\frac{R_p}{d}}\right) = \left[\frac{\rho_p}{\rho_{D_0}}\left(\frac{1-\eta}{\eta}\right)+1\right]^{1/3} \tag{80}$$

Equation (79) indicates that, in terms of the payload fraction, the spherical curvature ratio R_p/d is independent of the impact limiter mass.

Using Eq. (58) as the basis for developing the maximum impact velocity V_0 as a function of the payload fraction and the limiter constants, it is evident that the maximum impact velocity is a function of, among other things, the Dovetail weight density $\rho_{D(\phi,\theta)}$. However, $\rho_{D(\phi,\theta)}$ as given by Eq. (14) can be reworked to eliminate the Dovetail weight W_D.

Substituting Eq. (75) in Eq. (78) and the resulting equation in Eq. (14) yields

$$\rho_{D(\phi,\theta)} = \frac{\left(\frac{1-\eta}{\eta}\right)\left(\frac{R_p}{d}\right)\rho_p}{\left\{\left(1+\frac{1}{\frac{R_p}{d}}\right)\left(\frac{\cos\theta}{\cos\phi}\right)\left[\left(1+\frac{1}{\frac{R_p}{d}}\right)\left(\frac{\cos\theta}{\cos\phi}\right)+1\right]+1\right\}} \tag{81}$$

Substituting Eqs. (79) and (80) in Eq. (81) results in the following Dovetail density equation that is independent of weight:

$$\rho_{D(\phi,\theta)} = \frac{\left(\frac{1-\eta}{\eta}\right)\rho_p}{\left\{\left[\frac{\rho_p}{\rho_{D_0}}\left(\frac{1-\eta}{\eta}\right)+1\right]^{1/3}-1\right\}\left\{\left[\frac{\rho_p}{\rho_{D_0}}\left(\frac{1-\eta}{\eta}\right)+1\right]^{1/3}\left(\frac{\cos\theta}{\cos\phi}\right)\left(\left[\frac{\rho_p}{\rho_{D_0}}\left(\frac{1-\eta}{\eta}\right)+1\right]^{1/3}\left(\frac{\cos\theta}{\cos\phi}\right)+1\right)+1\right\}} \tag{82}$$

Now by substituting Eqs. (75), (78), (79), and (80) in Eq. (58) and rearranging terms, the maximum impact velocity can be expressed as shown in Eq. (83) on page 15.

Since it has been shown in Eq. (82) that the Dovetail density is independent of weight, it is evident upon elimination of the payload radius terms in Eq. (83) that the maximum impact velocity is independent of weight.

Also, it can be seen that the impact limiter deceleration, as given by the bracketed term "A" of Eq. (83), varies inversely with the payload radius. Cubing the bracketed term "A" and then multiplying by the total limiter weight results in an expression that is a function only of the payload fraction and the limiter constants. Letting W_0 be the total limiter weight, i.e., $W_0 = W_p + W_D$, and the value of the bracketed term "A" be N, the following relationship can be formed:

$$\psi = W_0 N^3 \tag{84}$$

By the definition of the payload fraction and the use of Eqs. (75) and (83), Eq. (84) may be rewritten as

$$\psi = \frac{W_p}{\eta}N^3 = \frac{4\pi R_p^3}{3\eta}\rho_p\underbrace{\left[\left(\frac{1}{R_p}\right)^3\{\cdots\}^3\right]}_{N^3} \tag{85}$$

Since the payload radius terms cancel out of the expression for ψ, it is evident that Eq. (85) is independent of limiter weight. Letting N be the maximum limiter deceleration $\ddot{x}_L$ (number of gs), it follows that ψ represents a parameter for maximum deceleration that will vary as a function of the payload fraction for a given set of limiter constants. Through the use of Eq. (85), levels of constant maximum deceleration can be developed as a function of the payload fraction and the limiter constants representing different design cases.

In a similar manner, a parameter for the maximum "cannonball" deceleration can be developed that is a function of the payload fraction and the limiter constants. Substituting Eq. (75) in Eq. (74) and expressing the resulting maximum deceleration equation in number of gs yields

$$N_{p_{MAX}} = \frac{3\sigma_{C_i}}{2R_p}\int_0^{\pi/2}\xi_{(\phi)}\sin\phi\,d\phi \tag{86}$$

Then, as before

$$\psi_p = W_0 N_{p_{MAX}}^3 = \frac{9\pi\sigma_{C_i}^3}{2\eta}\rho_p\left[\int_0^{\pi/2}\xi_{(\phi)}\sin\phi\,d\phi\right]^3 \tag{87}$$

For the same payload fraction and impact limiter constants, Eqs. (87) and (85) can be compared to determine if payload penetration can occur for the limiter design under consideration. Payload penetration will not occur provided

$$\frac{\psi_p}{\psi} > 1$$

To determine the total limiter radius as a function of the payload fraction and the limiter constants, use is made of Eq. (76). Noting that the total limiter radius R_0 can be expressed as the sum of the payload radius and Dovetail core depth, Eq. (76) can be rewritten as

$$R_0^3 = \frac{3W_D}{4\pi\rho_{D_0}} + R_p^3 \tag{88}$$

But, from the definition of the payload fraction, the following expression can be formed:

$$\psi_R = \frac{R_0^3}{W_0} = \frac{3(1-\eta)}{4\pi\rho_{D_0}} + \frac{3\eta}{4\pi\rho_p}$$

$$\therefore \psi_R = \frac{3}{4\pi\rho_{D_0}}\left[\left(\frac{\rho_{D_0}}{\rho_p}-1\right)\eta+1\right] \tag{89}$$

$$V_0^2 = 2R_p g\left[\frac{\rho_p}{\rho_{D_0}}\left(\frac{1-\eta}{\eta}\right)+1\right]^{1/3}$$

$$\times \int_0^{\theta_{MAX}} \overbrace{\left[\left(\frac{1}{R_p}\right)\left\{\left(\frac{2}{3}\frac{\rho_p}{\eta} - \frac{\rho_p\left(\frac{1-\eta}{\eta}\right)\left[\frac{\rho_p}{\rho_{D_0}}\left(\frac{1-\eta}{\eta}\right)+1\right]}{\left[\frac{\rho_p}{\rho_{D_0}}\left(\frac{1-\eta}{\eta}\right)+1\right]^{1/3}-1}\right)\int_0^{\theta}\sin\theta\cos^2\theta\int_0^{\theta}\frac{\tan\phi\sec^2\phi}{\left\{\left[\frac{\rho_p}{\rho_{D_0}}\left(\frac{1-\eta}{\eta}\right)+1\right]^{1/3}\left(\frac{\cos\theta}{\cos\phi}\right)\left(\left[\frac{\rho_p}{\rho_{D_0}}\left(\frac{1-\eta}{\eta}\right)+1\right]^{1/3}\left(\frac{\cos\theta}{\cos\phi}\right)+1\right)+1\right\}}d\phi\,d\theta \right.\right.}^{\text{A}}$$

$$\left.\left. \frac{\left[\frac{\rho_p}{\rho_{D_0}}\left(\frac{1-\eta}{\eta}\right)+1\right]^{2/3}\int_0^{\theta}\sigma_{0_{(\phi,\theta)}}\xi_{(\phi)}\left(\frac{\cos^2\theta\sin\phi}{\cos^3\phi}\right)d\phi}{} \right\}\right]$$

$$\times \sin\theta\, d\theta \tag{83}$$

Equation (89) shows that, independent of limiter weight, the total limiter radius parameter ψ_R varies linearly with the payload fraction for a given set of limiter constants. As in the case of maximum limiter deceleration, levels of constant limiter radius can be developed for design purposes.

From Eqs. (83), (85), (87), (89), (30), and (28), it is seen that the parameters affecting the design relations include η, ρ_p, ρ_{D_0}, t_f, L_D, $\bar{y}_0$. However, since the Dovetail foil thickness and weight density are synonymous, it is possible to develop a relationship between the foil thickness and the weight density of the Dovetail at the outer limiter surface, thereby reducing the number of design parameters by one. This relationship is presented in the following section.

2. *Dovetail foil thickness–spherical outer density relation.* The density at the outer surface can also be defined as the weight of a single Dovetail cell divided by the volume of that cell, that is,

$$\rho_{D_0} = \frac{w_C}{V_C} \tag{90}$$

Since the Dovetail is composed of phenolic resin built up on a glass cloth core, the weight of a single cell (neglecting the weight of the node bond adhesive) can be expressed as

$$w_C = w_G + w_p \tag{91}$$

where

w_G = weight of glass cloth in one cell

w_p = weight of phenolic resin in one cell

Now

$$w_G = \gamma_G a_C \tag{92}$$

where

γ_G = unit weight per in.^{2} of glass cloth area

a_C = surface area of a Dovetail cell

Then, from Fig. 2, Eq. (92) may be written as

$$w_G = \gamma_G \left[2L_D + \frac{1}{2}(4kL_D) \right] d$$

$$\therefore w_G = 2\gamma_G L_D d(1 + k) \tag{93}$$

For the weight of the phenolic resin:

$$w_p = \gamma_p \left(\frac{t_f}{2} \right) [2L_D + 4kL_D]\, d$$

$$\therefore w_p = \gamma_p t_f L_D d(1 + 2k) \tag{94}$$

Substituting Eqs. (93) and (94) in Eq. (91) yields

$$w_C = 2\gamma_G L_D d(1 + k) + \gamma_p t_f L_D d(1 + 2k) \tag{95}$$

Now the Dovetail cell volume may be written as

$$V_C = \int_0^d a_{(\Delta)} d\Delta \tag{96}$$

Substituting Eq. (6) in Eq. (96) and integrating yields

$$V_C = \bar{y}_0 L_D R_p \left(1 + \frac{1}{\frac{R_p}{d}} \right) \left\{ \frac{2\bar{y}_0}{3L_D} \left[1 - \left(\frac{1}{1 + \frac{R_p}{d}} \right)^3 \right] + \frac{1}{2} \left[1 - \left(\frac{1}{1 + \frac{R_p}{d}} \right)^2 \right] \right\} \tag{97}$$

Substituting Eqs. (95) and (97) in Eq. (90) results in the following expression for the Dovetail density at the outer surface of the sphere:

$$\rho_{D_0} = \frac{2\gamma_G(1 + k) + \gamma_p t_f (1 + 2k)}{\bar{y}_0 \left(\frac{R_p}{d} \right) \left(1 + \frac{1}{\frac{R_p}{d}} \right) \left\{ \frac{2\bar{y}_0}{3L_D} \left[1 - \left(\frac{1}{1 + \frac{R_p}{d}} \right)^3 \right] + \frac{1}{2} \left[1 - \left(\frac{1}{1 + \frac{R_p}{d}} \right)^2 \right] \right\}} \tag{98}$$

Alternatively, substituting Eqs. (27), (79), and (80) in Eq. (98) and solving for t_f yields

$$t_f = \frac{1}{\gamma_p \left\{1 + 0.706\left[1 + \left(\frac{4\bar{y}_0}{L_D} - 1\right)^2\right]^{1/2}\right\}} \left[\left\{ \frac{\left[\frac{\rho_p}{\rho_{D_0}}\left(\frac{1-\eta}{\eta}\right) + 1\right]^{1/3} \bar{y}_0 \rho_{D_0}}{\left[\frac{\rho_p}{\rho_{D_0}}\left(\frac{1-\eta}{\eta}\right) + 1\right]^{1/3} - 1} \right\} \left(\left\{ \frac{2\bar{y}_0}{3L_D} \right\} 1 - \frac{1}{\left[\frac{\rho_p}{\rho_{D_0}}\left(\frac{1-\eta}{\eta}\right) + 1\right]} \right\} \right.$$

$$\left. + \frac{1}{2} \left\{ 1 - \frac{1}{\left[\frac{\rho_p}{\rho_{D_0}}\left(\frac{1-\eta}{\eta}\right) + 1\right]^{2/3}} \right\} - 2\gamma_G \left\{ 1 + 0.353\left[1 + \left(\frac{4\bar{y}_0}{L_D} - 1\right)^2\right]^{1/2} \right\} \right) \right] \tag{99}$$

IV. Comments

The analysis capability presented in this report is intended to provide a basis both for evaluating a proposed Dovetail spherical limiter design and for developing design charts useful in parametric studies. In utilizing the analysis capability care must first be taken to develop design configurations that do not exceed the physical limitations of a Dovetail honeycomb (Ref. 1).

Nomenclature

A_{CB} area at crushing boundary

a cross-sectional area of Dovetail cell

a_C surface area of Dovetail cell

c stress wave velocity along a centrally loaded Dovetail cell

d Dovetail core depth (thickness)

d_C crushing depth (thickness)

E_p modulus of elasticity of phenolic resin

F force at the crushing boundary

F_x force acting on system of particles

g gravitational constant

L_D honeycomb land dimension

M_x linear momentum of system of particles in X direction

m_{UC} uncrushed mass of impact limiter

P general particle within control volume

P_C compressive force acting on payload below equator

Q general point on control volume boundary

R_p payload radius

R_0 total limiter radius

S system of particles

T total limiter stopping time

t time

t_f Dovetail cell foil thickness

u velocity of mass transfer boundary

V impact limiter velocity

V_i initial contact velocity

V_0 maximum impact velocity

$\bar{V}$ control volume

$\bar{V}_C$ crushed volume of sphere

v particle velocity

W_C Dovetail honeycomb crushed weight

W_D Dovetail total weight

W_p payload total weight

W_0 total impact limiter weight

w_G weight of glass cloth in one cell

Nomenclature (contd)

w_p	weight of phenolic resin in one cell
x	height of limiter CG above crushing surface
x_{CB}	height of limiter crushing boundary above crushing surface
$\dot{x}$	impact limiter velocity
$\ddot{x}_L$	maximum Dovetail deceleration
$\ddot{x}_p$	payload deceleration
$\bar{y}_0$	maximum Dovetail expansion
β	thickness efficiency
γ_G	unit weight per in.^{2} of glass cloth area
γ_p	weight density of phenolic resin
Δ	length of general Dovetail cell
η	limiter payload fraction
θ	ϕ_{max}
ξ	off-axis crushing stress reduction parameter
ρ	particle mass density
ρ_D	Dovetail weight density
ρ_{D_0}	Dovetail weight density at spherical outer surface
ρ_p	payload weight density
σ_{CB}	Dovetail crushing stress at crushing boundary
σ_{C_i}	axial crushing stress of Dovetail at payload-Dovetail interface
σ_{C_0}	axial crushing stress of Dovetail at outer surface
σ_0	general axial crushing stress of Dovetail
ϕ	angular location of general Dovetail cell

References

1. *Development of Energy-Dissipating Plastic Honeycomb,* Final Report No. 68 SD 4264 (prepared for JPL under Contract No. 951172). General Electric Co., Space Technology Center, Valley Forge, Pa., June 14, 1968.
2. *RF Transparent, Energy Absorbing, Structural Elements,* Phases I and II, Final Report Nos. 64 SD 565 and 64 SD 4329 (prepared for JPL under Contract No. 950564). General Electric Co., Space Technology Center, Valley Forge, Pa., Mar. 16 and Aug. 17, 1964.
3. *Impact Technology Document: Volume I,* Publication No. U-3031 (prepared for JPL under Contract No. 950996). Aeroneutronic Division of Philco Corporation, Newport Beach, Calif., Feb. 25, 1965.
4. Housner, G., and Hudson, D., *Applied Mechanics-Dynamic,* Second Edition. D. Van Nostrand Co., Inc., New York, Aug. 1959.
5. Timoshenko, S., *Theory of Elasticity,* First Edition. McGraw-Hill Book Co., Inc., New York, 1934.